Turbulence Spectra in the Atmospheric Surface Layer Using REAL and Doppler Lidars

Chenning Tong [(a)], Kirill Barskov [(a)], Pierre Dérian [(b)] and Shane D. Mayor [(b)]
[(a)] Clemson University
Department of Mechanical Engineering, Fluor Daniel Building, Clemson, SC 29634, USA
[(b)] California State University Chico
Department of Earth and Environmental Sciences, 400 W. 1st St., Chico, California, 95929, USA
Lead Author e-mail address: ctong@clemson.edu

Abstract: We report on ring-integrated horizontal velocity variance spectra in the atmospheric surface layer calculated from in situ measurements and two horizontally directed lidar systems. The spectra are used to test the multipoint Monin-Obukhov Similarity Theory (MMO).

1. Introduction

The theoretical foundation for the atmospheric surface layer, the Monin-Obukhov similarity theory (MOST) [1], is widely used but has long been recognized to have important deficiencies. The Multipoint Monin-Obukhov similarity theory (MMO) has been developed to address these deficiencies [2, 3]. In particular, it predicts the horizontal turbulence spectra for scales larger than the height from the ground.

MMO's spectral similarity scaling is formulated in terms of the 2D horizontal wavenumber magnitude. To validate MMO, ring-integrated spectra, which is obtained by integrating spectral power over all horizontal directions at a given wavenumber magnitude, are needed. By contrast, a 1D spectrum samples only one wavenumber component and can misrepresent the contributions to variance across spatial scales. However, ring-integrated spectra are more difficult to obtain because they require 2D velocity fields over a contiguous horizontal area, rather than a single transect needed for 1D spectra.

2. M2HATS

We conducted a field experiment named Multipoint MOST Horizontal Array Turbulence Study (M2HATS) [4] to test MMO. The experiment was conducted in a broad, nearly flat, and arid valley near Tonopah, Nevada, from July through September of 2023. In addition to several vertical profiling systems to observe the depth of the atmospheric boundary layer, we deployed multiple observing systems to observe the horizontal turbulence structure in the atmospheric surface layer. This included a linear array of 50 sonic anemometers, a horizontally staring Doppler lidar, and the horizontally scanning REAL.

3. Horizontal linear array

An array of 50 CSAT3 sonic anemometers was set up in a line perpendicular to the prevailing wind direction. The anemometers were spaced every 5 m in distance at 4 m above ground level (AGL). Therefore, the total horizontal span of the linear array was 245 m wide.

4. Doppler lidar

A Metek Halo Doppler lidar (serial #162) was installed on an elevated platform atop a shipping container at about 4 m ALG. Its wavelength was 1.55 microns, and it transmitted 40 microjoule pulses at 10 kHz. Its beam was held stationary and directed along a line close to, and almost parallel to, the linear array to provide a wider perspective of the velocity field moving through the linear array. It produced a range-versus-time array of radial velocity components with a 30 m gate spacing. The temporal resolution of the data was 1 second.

5. REAL

The original Raman-shifted Eye-safe Aerosol Lidar (REAL) [5-8], developed at the NCAR Earth Observing Laboratory from 2002-2007, was deployed to collect horizontal scans of elastic backscatter and 2D vector flow fields in the atmospheric surface layer. The transmitter employs a powerful Nd:YAG laser and a high-pressure gas cell to generate 130 mJ pulses at 1.54 microns wavelength through stimulated

Raman scattering in methane. The pulses are 6 ns in duration at 10 Hz. The receiver includes a 40 cm diameter Newtonian telescope and two InGaAs avalanche photodiodes for polarization sensitivity. The data acquisition system uses a 2-channel analog-to-digital converter with 14-bit resolution sampling at 100M samples per second for 1.5 m radial resolution of aerosol backscatter.

The REAL is housed in a mobile facility consisting of two 20-foot (6 m) long shipping containers on a 48-foot (14.6 m) long flatbed trailer. When deployed, the platform stands firmly upon 4 manually adjustable leveling legs. High-precision, high-accuracy tiltmeters constantly measure the attitude of the optics table. The laboratory container on the front of the trailer is temperature-stabilized, HEPA-filtered, and it has large uninterruptible power supplies to maintain operation through challenging field conditions. A rooftop scanner permits full hemispherical scanning.

6. Typhoon

Typhoon [9] is software that applies a wavelet-based motion estimation algorithm to consecutive pairs of 2D images. As a global method, it solves for the displacement of aerosol image features simultaneously in the entire domain, whereas local methods such as cross-correlation [10] break the motion field estimation into many independent sub-problems. Typhoon also provides a dense solution, which is a displacement vector at every pixel. The flow field is estimated by minimizing a functional which combines a data model and a regularization term. A user-defined parameter balances the two terms. Typhoon is written in C/C++ with calls to CUDA to perform the calculation in a massively parallel fashion in real-time. It runs on a Linux server with Nvidia GPUs inside the REAL laboratory container.

Before applying Typhoon, the REAL backscatter data is first range-corrected and band-pass median-filtered, then interpolated from its native polar coordinate system with $\Delta r = 1.5$ m and $\Delta\theta = 0.4°$ to a Cartesian coordinate system with an arbitrary resolution, chosen for this project to be $\Delta x = \Delta y = 8$ m. The wind estimation is restricted to the regions of the scan containing coherent aerosol features, and the process corrects for image distortions due to the lidar scanning motion [11].

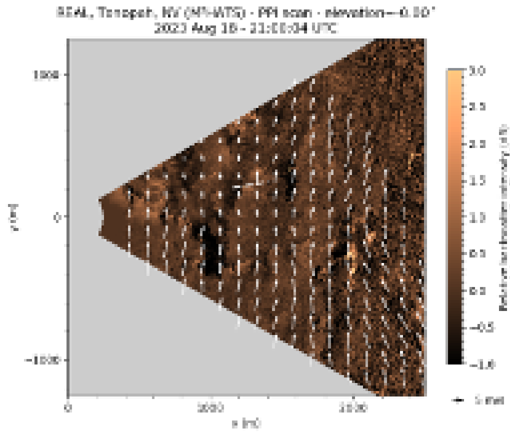

Figure 1. A single vector flow field derived from two consecutive scans of the REAL using the Typhoon motion estimation algorithm during M^{2}HATS. Vectors shown are a subset of the full-resolution field derived by Typhoon. The white dashed line indicates the position of the 250-m wide linear array of sonic anemometers.

Over 629 hours of REAL data (about 153,000 scans, 0.8 TB) were collected over a wide range of meteorological conditions. The derived vector flow fields amount to about 26 GB. Because of the importance of unstable daytime conditions, we typically operated the REAL from morning until evening. While the REAL almost always detected useful backscatter signal to at least 2 km range, the aerosol conditions were challenging for lidars in that (a) the air was often very low humidity, high visibility, and not contaminated by human-made sources of pollution, and (b) ideal conditions for motion estimation only occurred when the wind speed was strong enough to lift naturally occurring dust from the surface.

7. Calculation of Spectra and Results

Each of the observing systems discussed above has strengths and weaknesses in providing desirable velocity data. The sonic anemometer data have exquisite resolution and 3 orthogonal components, but are limited to a span of 245 m and, in fact, are observations of velocity on a line. By invoking Taylor's hypothesis, we may convert time to a second spatial dimension. The fixed-beam Doppler lidar produces accurate velocity measurements, but it is also restricted to a line, lower resolution, and only includes the radial comp. The REAL/Typhoon approach provides 2-component vector flow fields, but lacks the spatial and temporal resolution of the other systems.

The spectra of the *u*- (streamwise) and *v*- (transverse) wind components are obtained from the REAL/Typhoon results. The REAL frames are cross-checked with the horizontal Doppler lidar data and sonic array data to select only the relevant scanning frames. Each frame is rotated based on the wind direction obtained from the anemometer array for the selected stationary time interval so that the x-axis is aligned with the mean wind. The largest square area is selected from each rotated frame. Two-dimensional spectra and the corresponding ring-integrated spectra are calculated for each square area. The ring-integrated spectra are then averaged over the entire stationary time interval.

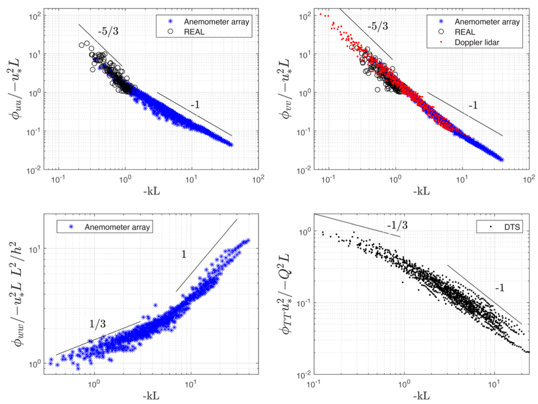

Figure 2: Velocity spectra measured by sonic anemometers array, Doppler lidar and the REAL, and temperature spectrum measured by a distributed temperature system. The spectra obtained by REAL are only shown for $k < 0.03$ m^{-1} as higher wavenumbers are rolled off due to its spatial resolution of approximately 100 m.

The two-component velocity fields obtained using REAL/Typhoon have an effective spatial resolution of approximately 100 m; therefore, wavenumbers larger than $k \approx 0.03$ m^{-1} are not included in the analysis.

The spectrum of the *v*-component was also obtained using the Halo Doppler lidar. An initial quasi-two-dimensional *v*-field is obtained using Taylor's frozen field hypothesis for each stationary interval. The first 120 m of data from the lidar is excluded from the analysis to avoid the influence of the structures near the lidar. The data for large ranges are also excluded because of low backscatter signal and high noise levels. The range containing signals of good quality is identified for each beam using values of *v* and the derivatives of the velocity field in different directions, with high signal-to-noise-ratio data used as a reference for the considered time interval.

The data from the ultrasonic anemometer array placed along the lidar beam are used for additional calibration of the Doppler lidar velocity. The velocity field is rotated based on the wind direction obtained from the sonic array so that the x-axis is aligned with the mean wind. The rotated velocity field is divided into square areas with no more than 50% overlap. Squares smaller than 400 m are excluded from the analysis. Two-dimensional spectra are calculated for each square separately.

Attenuation of the Doppler lidar spectra due to spatial averaging along the beam (30 m spatial resolution) and temporal averaging (over several integration periods) is corrected by dividing by the sinc transfer function of the averaging filter. The ring-integrated spectra are obtained from each two-dimensional spectrum and averaged over the entire stationary time interval. The ring-integrated spectra are compared with the MMO prediction. The ring-integrated *u*- and *v*-spectra have a $k^{-5/3}$ dependence for the convective range ($1/z_i < k < -1/L$) and a k^{-1} dependence for the dynamic range ($-1/L < k < 1/z$), where L is the Obukhov length, which separates the buoyancy- and shear-dominated scales. Figure 2 shows the *u*- and *v*-spectra. The MMO prediction agrees with the data. The REAL data resolves well the convective range, while the sonic anemometer array covers the highest wavenumber portion of the convective range and the dynamics range. For the *v*-spectrum, the Doppler lidar also resolves the convective range and a small portion of the dynamics range.

We also include the *w*- and temperature (T) spectra in Figure 2. The former is calculated using the sonic array alone and the latter using a fiber optic. The *w*-spectrum agrees with the prediction of $k^{\frac{1}{3}}$ and k^{1} scaling for the two ranges. The data agrees with the prediction, offering a consistency check for the array. The temperature spectrum also agrees with the predicted $k^{-\frac{1}{3}}$ and k^{-1} scaling, further demonstrating the consistency of the MMO prediction with the field measurement data.

8. Conclusions

We used the REAL and a Doppler lidar to measure the ring-integrated horizontal velocity spectra. The former can resolve scales down to 100 m, while the latter has a resolution of 30 m. The agreement of the data with the MMO prediction demonstrates the capability of these instruments to resolve turbulence structures in the atmospheric boundary layer.

9. Acknowledgements

M2HATS and this work were supported by NSF AGS-2054983 and AGS-2054969. NCAR Earth Observing Laboratory provided critical field support and data processing.

10. References

[1] Monin, A. S. and A. M. Obukhov, “Basic laws of turbulent mixing in the ground layer of the atmosphere,” Tr. Geofiz. Inst., Akad. Nauk SSSR, **24**, 163-187 (1954).

[2] Tong, C. and K. X. Nguyen, “Multipoint Monin-Obukhov similarity theory and Its Application to Turbulence Spectra in the Convective Atmospheric Surface Layer,” J. Atmos. Sci., **72**, 4337-4348 (2015).

[3] Tong, C. and M. Ding, “Multi-point Monin-Obukhov similarity in the convective atmospheric surface layer using matched asymptotic expansions,” J. Fluid Mech., **864**, 640-669 (2019).

[4] Tong, C. et al., “Multipoint Monin-Obukhov Similarity Theory Horizontal Array Turbulence Study (M2HATS), Accepted, Bull. Am. Meterol. Soc. (2026)

[5] Mayor, S. D. and S. M. Spuler, “Raman-shifted eye-safe aerosol lidar,” Appl. Optics, **43**, 3915-3924 (2004).

[6] Spuler, S. M. and S. D. Mayor, “Scanning Eye-Safe Elastic Backscatter Lidar at 1.54μm,” J. Atmos. Ocean. Tech., **22**, 696-703. (2005).

[7] Mayor, S. D., S. M. Spuler, B. M. Morley, E. Loew, “Polarization lidar at 1.54-microns and observations of plumes from aerosol generators,” Opt. Eng., **46**, 096201 (2007).

[8] Spuler, S. M. and S. D. Mayor, “Raman shifter optimized for lidar at a 1.5 μm wavelength,” Appl. Optics, **46**, 2990-2995 (2007).

[9] Dérian, P., C. F. Mauzey, and S. D. Mayor, “Wavelet-based optical flow for two-component wind field estimation from single aerosol lidar data,” J. Atmos. Ocean. Technol., **32**, 1759-1778 (2015).

[10] Hamada, M., P. Dérian, C. F. Mauzey, and S. D. Mayor, “Optimization of the Cross-Correlation Algorithm for Two-Component Wind Field Estimation from Single Aerosol Lidar Data and Comparison with Doppler Lidar,” J. Atmos. Ocean. Technol.}, **33**, 81-101 (2016).

[11] Sasano, Y., H. Hirohara, T. Yamasaki, H. Shimizu, N. Takeuchi, and T. Kawamura, “Horizontal wind vector determination from the displacement of aerosol distribution patterns observed by a scanning lidar,” J. Appl. Meteor., **21**, 1516-1523 (1982).